RESEARCH ARTICLE | MAY 03 2021

Electron mobility anisotropy in InAs/GaAs(001) heterostructures

Son Phuong Le ; Toshi-kazu Suzuki

Appl. Phys. Lett. 118, 182101 (2021)
https://doi.org/10.1063/5.0039748

Applied Physics Letters ARTICLE scitation.org/journal/apl

Electron mobility anisotropy in InAs/GaAs(001) heterostructures

Cite as: Appl. Phys. Lett. **118**, 182101 (2021); doi: 10.1063/5.0039748
Submitted: 6 December 2020 · Accepted: 18 April 2021 ·
Published Online: 3 May 2021

Son Phuong Le[1,a] and Toshi-kazu Suzuki[2]

AFFILIATIONS

[1]Department of Physics, Chemistry and Biology, Linköping University, SE 581-83, Linköping, Sweden
[2]Center for Nano Materials and Technology, Japan Advanced Institute of Science and Technology (JAIST), 1-1 Asahidai, Nomi, Ishikawa 923-1292, Japan

[a]Author to whom correspondence should be addressed: son.le@liu.se

ABSTRACT

Electron transport properties in InAs films epitaxially grown on GaAs(001), InAs/GaAs(001) heterostructures, were systematically investigated through the dependence on crystal direction, thickness, and temperature. As a result, we found a pronounced electron mobility anisotropy, in which the mobility is highest and lowest along $[1\bar{1}0]$ and [110] crystal directions, respectively. The mobility anisotropy intensifies as the InAs thickness decreases, while it diminishes in thick regimes, where the InAs films are relatively immune to effects from the epitaxial heterointerface. We observed the anisotropy in a wide temperature range, 5–395 K, with an enhancement at high temperatures. Our analysis indicates that the electron mobility anisotropy can be attributed to anisotropic electron scatterings by both interface roughness and random piezoelectric polarization near the interface.

InAs, a narrow-gap compound semiconductor with attractive physical properties,[1,2] is promising for high-performance applications such as mid-infrared optical devices,[3] ultra-high-speed electron devices,[4–6] and also interband tunnel devices.[7,8] Heterogeneous integration of InAs thin films on host substrates has been reported with excellent device performances.[9–13] However, InAs films directly grown on GaAs are more accessible and are again drawing research attention,[14–16] although the crystal quality of the InAs/GaAs is a concern.[17] In the InAs/GaAs, crystal imperfections near the heterointerface due to the large lattice mismatch between InAs and GaAs cause electron scattering dominating electron transport properties. Such interface-related scattering can be an origin of anisotropic electron mobilities, which are sometimes observed in (In)GaAs channel heterostructures at low temperatures[18–25] and are attributed to anisotropic interface roughness,[18] cross-hatch morphology,[21] lattice relaxation,[19] dislocation distribution,[24,25] composition modulation,[22] and random piezoelectricity.[23] However, there is no study on the mobility anisotropy in InAs/GaAs heterostructures as well as its dependences on the InAs thickness and temperature. In this work, using InAs films epitaxially grown by molecular beam epitaxy (MBE) on GaAs(001) substrates, we investigated electron transport properties in InAs/GaAs(001) and their dependences on crystal direction, film thickness, and temperature. As a result, we found an electron mobility anisotropy, which increases with decreasing InAs thickness, in the whole measured temperature range of 5–395 K including a temperature-enhanced behavior at high temperatures. The electron mobility anisotropy was analyzed and attributed to anisotropic electron scatterings by both interface roughness and random piezoelectric (PE) polarization near the interface.

Undoped InAs film layers were grown by means of solid-source MBE on semi-insulating GaAs(001) substrates at 480 °C with a growth rate on the order of 1 ML/s in an arsenic-rich atmosphere. After the growth, InAs surfaces were examined by atomic force microscope (AFM). We fabricated 6-terminal Hall-bar devices (50 μm width and 200 μm length) with eight current-flowing directions for the InAs/GaAs(001) having InAs thickness $d \sim$ 10 nm– $\sim \mu$m, where InAs layer isolation and thinning were carried out by wet etching. Figure 1(a) shows an example of the AFM surface images, which has a roughness root mean square (RMS) of 3.6 nm, and cross-hatch morphology (CHM) is not exhibited.[26] The CHM is sometimes associated with electron mobility anisotropy in InGaAs systems.[19,21,22,24,25] However, such mobility anisotropy is sometimes observed in the systems without CHM.[20,23] In addition, some InGaAs systems with clear CHM do not show a notable mobility anisotropy,[27] implying other origin(s) of the observed mobility anisotropy. The device fabrication process, including the isolation and thinning, and electrode formation, is schematically shown in Fig. 1(b). The current-flowing directions

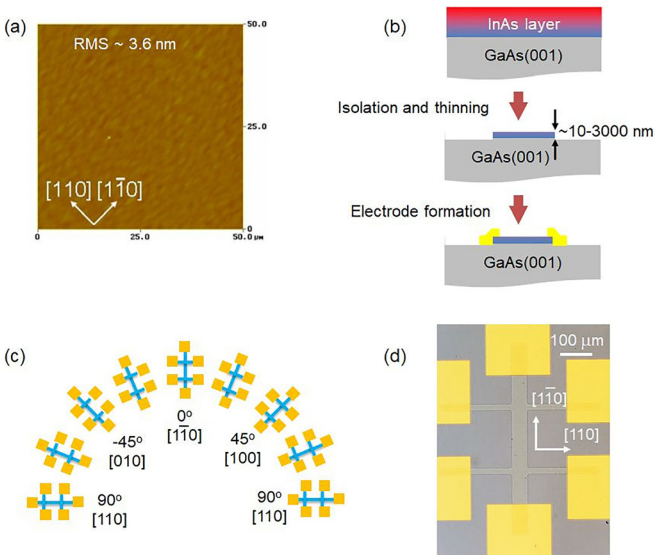

FIG. 1. (a) An AFM image of InAs surfaces, (b) the schematic of fabrication process, (c) an illustration of current flowing direction, and (d) an optical image of Hall-bar devices.

with angles θ from the $[1\bar{1}0]$ crystal direction are given in Fig. 1(c). An optical image of a Hall-bar device is shown in Fig. 1(d). The electron mobility μ and the sheet electron concentration n_s in the InAs/GaAs(001) were obtained by Hall-effect measurements under a magnetic field of 0.32 T. For temperature dependence of transport properties, a liquid-helium-type cryostat was employed for the measurements from 5 K to 395 K under the same magnetic field.

Hall-effect measurement results at room temperature are shown in Fig. 2 as functions of θ with some spotted InAs thicknesses. As seen in the inset, n_s exhibits almost constant values for every film thickness, i.e., isotropic behavior on the order of 10^{12} cm^{-2}. In spite of the undoped InAs layers, we do not observe electron depletion even for very thin InAs films, owing to the Fermi level pinning above the conduction band bottom,[28,29] where the electrons are distributed through the film thickness as shown in Ref. 30. On the other hand, we recognize anisotropic mobilities, θ-dependent μ, as obviously noticed in Figs. 2(a) and 2(b) showing the inverse mobility $1/\mu$ in full-scale and multi-panel plots, respectively. The highest electron mobility is along $[1\bar{1}0]$ crystal direction corresponding to $\theta = 0°$, and the lowest is along [110] direction with $\theta = 90°$, while intermediate values are through other directions, e.g., $\theta = \pm 45°$. The total electron mobility μ can be expressed by a Matthiessen form

$$\frac{1}{\mu} = \frac{1}{\mu_0} + \frac{f(\theta)}{\tilde{\mu}}, \tag{1}$$

where μ_0 and $\tilde{\mu}$ are mobility components in the θ-independent and θ-dependent terms, respectively, and $f(\theta)$ is an even function of θ satisfying $f(0°) = 0$ and $f(90°) = f(-90°) = 1$, which will be examined later. In Fig. 2(b), $1/\mu_0$ and $1/\tilde{\mu}$ schematically defined. It should be noted that $\mu_{[1\bar{1}0]} = \mu_0$ and $\mu_{[110]} = \mu_0\tilde{\mu}/(\mu_0 + \tilde{\mu})$, leading to $\mu_{[1\bar{1}0]}/\mu_{[110]} = 1 + \mu_0/\tilde{\mu}$.

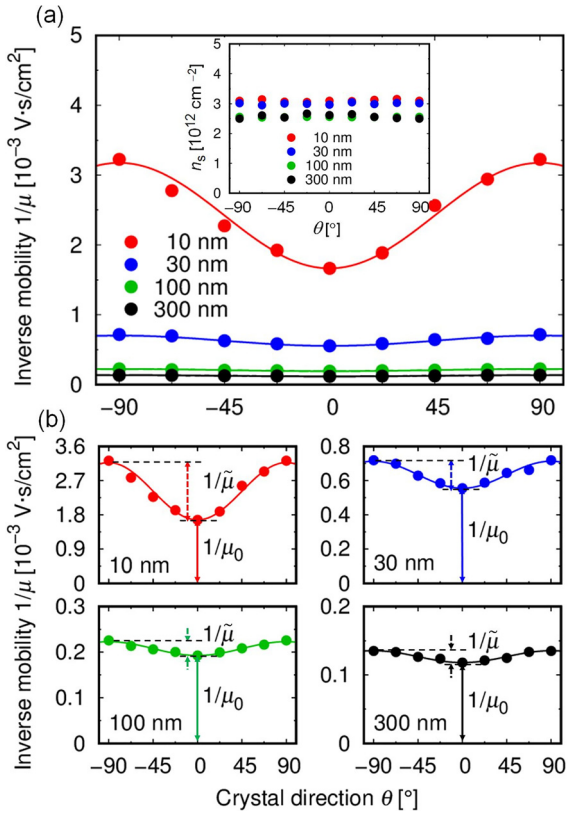

FIG. 2. The inverse room-temperature electron mobility $1/\mu$ as functions of the crystal direction θ for InAs/GaAs(001) in (a) full-scale and (b) multi-panel plots. The inset: The room-temperature sheet electron concentration n_s as functions of the crystal direction θ for InAs/GaAs(001).

Despite no clear thickness dependence of n_s, μ decreases with decreasing InAs thickness d, owing to high-density crystal defects near the InAs/GaAs interface.[26] The electrons occupy several subbands, whose mobilities are averaged to give the measured mobility. For subband wave functions extended through the thickness, as in thin layers $\lesssim$100 nm,[30] the electron average position is $\sim d/2$ from the interface. Thus, each subband has several scattering times (corresponding to mechanisms) as functions of d, accordingly a mobility as a function of d. For thick layers, interface and surface accumulation subbands exist; the former with an extremely low mobility gives minute contribution to the measured high mobility of a thick layer, and the latter has scattering times and a mobility depending on d. Therefore, hereafter, we discuss the measured mobility as a function of d. In Fig. 3(a), $1/\mu_0$ and $1/\tilde{\mu}$ as functions of d are shown, exhibiting monotonic decrease for both μ_0 and $\tilde{\mu}$ with decreasing d. In addition, the contribution of $\tilde{\mu}$ to the total mobility becomes more significant for thinner InAs films, i.e., the thinner film the stronger anisotropy. The fact that the anisotropy intensifies when the InAs film thickness decreases suggests that the observed mobility anisotropy is primarily caused by scattering mechanisms at/near the InAs/GaAs interface. The mobility ratio $\mu_{[1\bar{1}0]}/\mu_{[110]} = 1 + \mu_0/\tilde{\mu}$ at room temperature is shown in Fig. 3(b) as a function of the InAs film thickness for the InAs/GaAs(001), and also

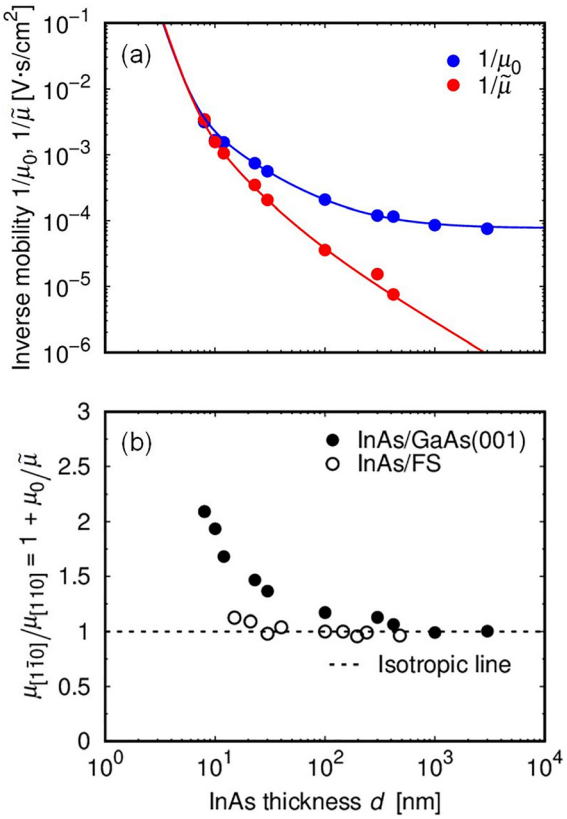

FIG. 3. (a) The inverse mobilities $1/\mu_0$, $1/\tilde{\mu}$ for InAs/GaAs(001), and (b) the mobility ratio $\mu_{[1\bar{1}0]}/\mu_{[110]} = 1 + \mu_0/\tilde{\mu}$ at room temperature as functions of the InAs thickness.

for InAs films bonded on low-k flexible substrate (InAs/FS).[13,30–32] The InAs/GaAs(001) shows a clear mobility anisotropy, i.e., $\mu_{[1\bar{1}0]}/\mu_{[110]} > 1$ for the thickness regime $\lesssim$30 nm, but the anisotropy alleviates as the thickness increases, and vanishes for very thick regimes $\gtrsim 1\,\mu$m. On the other hand, the InAs/FS, in which the InAs films are free from imperfections associated with the epitaxial heterointerface, exhibits negligible anisotropy for the whole measured thickness range. These results confirm that the observed mobility anisotropy in the InAs/GaAs(001) can be attributed to anisotropic scattering(s) associated with the InAs/GaAs(001) heterointerface.

Analyzing the thickness dependence of μ_0 and $\tilde{\mu}$ at room temperature, we find that the mobility components can be well fitted by Matthiessen forms

$$\frac{1}{\mu_0} = \frac{1}{\mu_{\rm in}} + \frac{A_0}{d^{5.2}} + \frac{B_0}{d^2} + \frac{C_0}{d}, \tag{2}$$

and

$$\frac{1}{\tilde{\mu}} = \frac{\tilde{A}}{d^{5.2}} + \frac{\tilde{B}}{d^2} + \frac{\tilde{C}}{d}, \tag{3}$$

as indicated by the fitting curves in Fig. 3(a), where $\mu_{\rm in}$ is a thickness-independent mobility, and the $d^{-5.2}$-proportional and d^{-1}-proportional terms, respectively, correspond to interface roughness (thickness fluctuation) scattering and Coulomb scattering by the interface charges,[30] while the d^{-2}-proportional terms will be examined later. The fitting gives a thickness-independent mobility $\mu_{\rm in} \simeq 13\,000$ cm^2/V s, which is owing to isotropic phonon scattering giving a mobility of $\sim$25 000 cm^2/V s,[33] and additional isotropic scattering independent of the thickness, such as bulk dislocation scattering. In thick InAs film regimes, this mobility dominates the total mobility, alleviating the mobility anisotropy. For $d^{-5.2}$-proportional and d^{-2}-proportional terms, we find $\tilde{A}/A_0 \simeq \tilde{B}/B_0 \sim 1$ from the fitting, suggesting that these terms have a related mechanism of the anisotropy. On the other hand, $C_0 \gg \tilde{C}$ holds for the d^{-1}-proportional Coulomb scattering, whose coefficient should be given by $(n_{\rm C}e^3m^{*2})/(4\pi\varepsilon_{\rm s}^2\hbar^3k_{\rm F}^3)$ using the interface charge density $n_{\rm C}$, the electron effective mass m^*, the dielectric constant $\varepsilon_{\rm s}$, and the Fermi wave vector $k_{\rm F}$.[13,30,31] From the value of C_0 obtained by the fitting, we find that the interface charges with a density $n_{\rm C} \sim 6 \times 10^{13}$ cm^{-2} causes nearly isotropic scattering, apart from a weak contribution from an anisotropic charge distribution giving a small $\tilde{C}$. Therefore, we consider that the essence of the anisotropic mobility is attributed to the $d^{-5.2}$-proportional and d^{-2}-proportional terms with a related mechanism of the anisotropy.

Owing to a large lattice mismatch, the InAs/GaAs(001) heterostructures possess large heterointerface roughness and random strain near the interface. In particular, there must be non-vanishing random shear strain, even though its average is zero. The strain induces PE polarization $\boldsymbol{P}$ given by

$$\boldsymbol{P} = \begin{pmatrix} P_x \\ P_y \\ P_z \end{pmatrix} = \begin{pmatrix} 0 & 0 & 0 & e_{14} & 0 & 0 \\ 0 & 0 & 0 & 0 & e_{14} & 0 \\ 0 & 0 & 0 & 0 & 0 & e_{14} \end{pmatrix} \begin{pmatrix} \varepsilon_{xx} \\ \varepsilon_{yy} \\ \varepsilon_{zz} \\ \varepsilon_{yz} \\ \varepsilon_{zx} \\ \varepsilon_{xy} \end{pmatrix}, \tag{4}$$

in the zinc blende InAs, where e_{14} is the PE constant and ε_{jk} is the strain tensor.[34,35] It should be noted that, only the off diagonal components of ε_{jk}, the shear strain components, contribute to the PE polarization. Thus, the non-vanishing random shear strain near the interface causes random PE polarization,[36–38] even though its average is zero. The random PE polarization scatters electrons via a random dipole potential, which is a square-inverse r^{-2} potential, whereas a Coulomb (monopole) potential is r^{-1}. While the Coulomb potential by the interface charges gives scattering probability $\propto d^{-1}$, the dipole potential by the random PE polarization will give scattering probability $\propto d^{-2}$. Therefore, we consider that the d^{-2}-proportional terms in (2) and (3) are attributed to the random PE polarization scattering, while the $d^{-5.2}$ and d^{-1} terms, respectively, to the interface roughness scattering and the Coulomb scattering. Both the interface roughness scattering and the random PE polarization scattering are associated with the heterointerface randomness,[36–38] where the randomness can be anisotropic; for example, can be intensified by misfit dislocations developing asymmetrically along [110] and [1$\bar{1}$0].[39–41] Thus, both the interface roughness scattering and the random PE polarization scattering can be anisotropic, leading to the electron mobility anisotropy. The mobility limited by the interface roughness scattering is $\mu_{\rm IR} \propto (\Delta\Lambda)^{-2} \exp(k_{\rm F}^2\Lambda^2) \sim (\Delta\Lambda)^{-2}$,[42] and that limited by the

random PE polarization scattering is $\mu_{PE} \propto (e_{14}\varepsilon\Delta\Lambda)^{-2} \exp(k_F^2\Lambda^2) \sim (e_{14}\varepsilon\Delta\Lambda)^{-2}$,[36–38] using the interface randomness amplitude Δ and correlation length Λ, and the average normal strain ε, where the last approximation is for small $k_F\Lambda$. It should be noted that the correlation length can be anisotropic. Assuming the randomness in the form of elliptical islands[18,43] with the width of $2\Lambda_0$ along the $[1\bar{1}0]$ direction and an eccentricity η, we obtain $\Lambda(\theta) = \Lambda_0/\sqrt{1-\eta^2\sin^2\theta}$, and thus

$$\mu_{IR}(\theta) = \mu_{IR0}(1-\eta^2\sin^2\theta), \tag{5}$$

and

$$\mu_{PE}(\theta) = \mu_{PE0}(1-\eta^2\sin^2\theta), \tag{6}$$

where $\mu_{IR0} \propto (\Delta\Lambda_0)^{-2}$ and $\mu_{PE0} \propto (e_{14}\varepsilon\Delta\Lambda_0)^{-2}$. These indicate that $f(\theta)$ in (1) should be given by

$$f(\theta) = \frac{(1-\eta^2)\sin^2\theta}{1-\eta^2\sin^2\theta}, \tag{7}$$

and $\tilde{A}/A_0$ and $\tilde{B}/B_0$ in (2) and (3) should be given by $\eta^2/(1-\eta^2)$. The fitting curve of μ using $f(\theta)$ shown in Fig. 2 gives $\eta \simeq 0.7$, leading to $\tilde{A}/A_0 \simeq \tilde{B}/B_0 \sim 1$. The good fitting supports the picture that the electron mobility anisotropy is attributed to both the anisotropic interface roughness scattering and the random PE polarization scattering.

Furthermore, the electron mobility μ as a function of temperature T is shown in Fig. 4(a) for some spotted InAs thicknesses. The mobility anisotropy is observed in whole measurement temperature range, 5–395 K, with the highest mobility along the $[1\bar{1}0]$ direction, the lowest along the [110] direction, and the intermediate through the [100] direction. As shown in Fig. 4(b), we obtain $1/\mu_0$ and $1/\tilde{\mu}$ as functions of T, exhibiting stronger temperature dependences for $\tilde{\mu}$ than for μ_0. Moreover, by plotting the ratio $\mu_{[1\bar{1}0]}/\mu_{[110]} = 1 + \mu_0/\tilde{\mu}$ as functions of T as shown in Fig. 5, we find a temperature-enhanced anisotropy at the high-temperature regimes, the higher temperatures the higher $\mu_{[1\bar{1}0]}/\mu_{[110]}$, i.e., the more dominant $\tilde{\mu}$. In the previous reports, mobility anisotropies were observed only at low temperatures, but not at high temperatures,[18–23] owing to isotropic phonon scattering dominating high-temperature mobilities. In contrast, we obtain the temperature-enhanced mobility anisotropy in the InAs/GaAs(001) at high temperatures. We consider that this behavior is attributed to temperature dependence of the mobility due to the anisotropic random PE polarization scattering, $\mu_{PE} \propto (e_{14}\varepsilon\Delta\Lambda)^{-2}$. Whereas Δ and Λ do not have temperature dependence as a matter of course, e_{14} or ε does. The average normal strain ε might be enhanced by an increase in temperature. Moreover, the PE constant e_{14} can strongly depend on temperature, as reported in Refs. 44–46; the higher T the larger e_{14}, i.e., the lower μ_{PE}. Hence, higher temperatures give more dominant anisotropic μ_{PE}, leading to the temperature-enhanced electron mobility anisotropy. A crude estimation gives that $\tilde{B}$ almost doubles with temperature increasing from 5 to 395 K, whereas $\tilde{A}$ and $\tilde{C}$ stay nearly constant, supporting the above picture. For the systems in Refs. 18–25, the lattice mismatch between the channel and the barrier is small, even though the buffer-substrate lattice mismatch is large in some cases, and the "metamorphic interface" is micrometers away from the channel. Accordingly, the random strain in the channel is small, and the random PE polarization is relatively weak. Therefore, the anisotropic random PE polarization scattering, if any, is smeared out by the isotropic phonon scattering at high temperatures. Similarly, the mobility

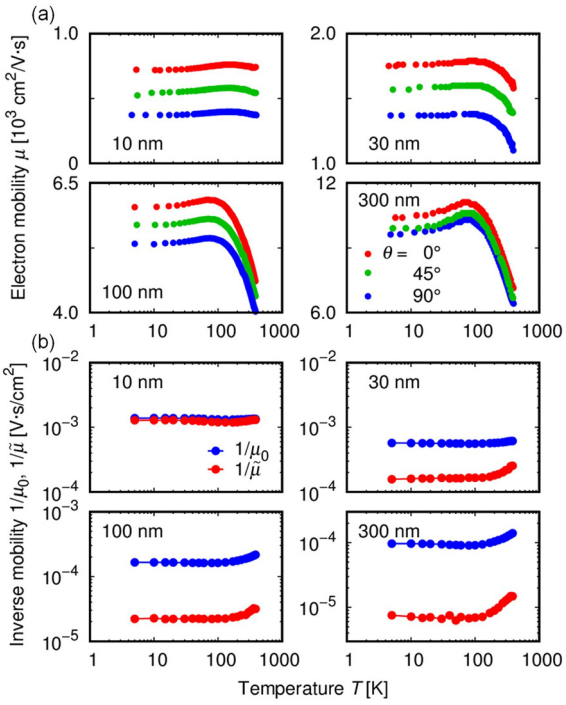

FIG. 4. Temperature dependence of (a) the electron mobility μ and (b) the inverse of its components $1/\mu_0$ and $1/\tilde{\mu}$ in InAs/GaAs(001).

anisotropy is not observed for the InAs/FS, not having such a lattice-mismatched interface with the anisotropic roughness and random PE polarization. This indicates that effects of the top etched InAs surface are not significant.

In summary, for lattice-mismatched InAs/GaAs(001) heterostructures with different InAs thicknesses, we investigated the dependence of electron transport properties on crystal directions in a wide temperature range. As a result, we found a pronounced electron mobility anisotropy, which is enhanced either in the thin InAs film

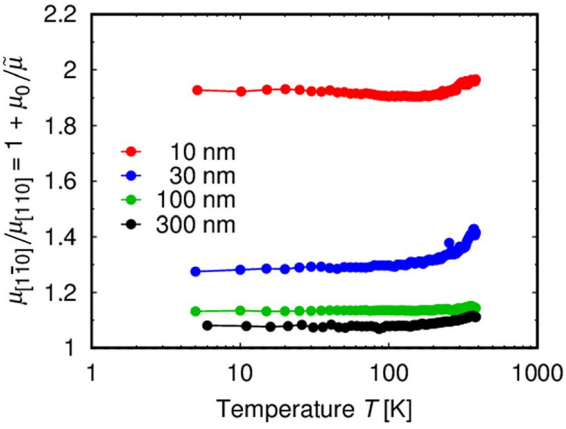

FIG. 5. Temperature dependence of the mobility ratio $\mu_{[1\bar{1}0]}/\mu_{[110]} = 1 + \mu_0/\tilde{\mu}$ for InAs/GaAs(001).

regimes or at high temperatures. From our analysis, it is concluded that the mobility anisotropy can be attributed to anisotropic electron scatterings by both interface roughness and random piezoelectric polarization near the interface. The anisotropic scatterings are associated with an anisotropy of the correlation length of the randomness of the heterointerface. The temperature-enhanced electron mobility anisotropy can be attributed to the random piezoelectric polarization. These insights are informative for physics of the electron transport in InAs/GaAs systems, and their device applications.

The authors would like to acknowledge the financial support from Energimyndigheten, Project No. 46671-1 (SPL), and from JSPS KAKENHI, Grant Nos. 26249046 and 15K13348 (TS).

DATA AVAILABILITY

The data that support the findings of this study are available from the corresponding author upon reasonable request.

REFERENCES

[1]A. Milnes and A. Polyakov, Mater. Sci. Eng., B **18**, 237 (1993).
[2]H. Kroemer, Physica E **20**, 196 (2004).
[3]Z. Yin and X. Tang, Solid-State Electron. **51**, 6 (2007).
[4]B. R. Bennett, R. Magno, J. B. Boos, W. Kruppa, and M. G. Ancona, Solid-State Electron. **49**, 1875 (2005).
[5]D.-H. Kim and J. del Alamo, IEEE Electron Device Lett. **31**, 806 (2010).
[6]N. Li, E. S. Harmon, J. Hyland, D. B. Salzman, T. P. Ma, Y. Xuan, and P. D. Ye, Appl. Phys. Lett. **92**, 143507 (2008).
[7]Q. Zhang, W. Zhao, and A. Seabaugh, IEEE Electron Device Lett. **27**, 297 (2006).
[8]M. Luisier and G. Klimeck, IEEE Electron Device Lett. **30**, 602 (2009).
[9]J. Shi, N. Wichmann, Y. Roelens, and S. Bollaert, Appl. Phys. Lett. **99**, 203505 (2011).
[10]H. Ko, K. Takei, R. Kapadia, S. Chuang, H. Fang, P. W. Leu, K. Ganapathi, E. Plis, H. S. Kim, S.-Y. Chen, M. Madsen, A. C. Ford, Y.-L. Chueh, S. Krishna, S. Salahuddin, and A. Javey, Nature **468**, 286 (2010).
[11]K. Takei, S. Chuang, H. Fang, R. Kapadia, C.-H. Liu, J. Nah, H. Sul Kim, E. Plis, S. Krishna, Y.-L. Chueh, and A. Javey, Appl. Phys. Lett. **99**, 103507 (2011).
[12]K. Takei, H. Fang, S. B. Kumar, R. Kapadia, Q. Gao, M. Madsen, H. S. Kim, C.-H. Liu, Y.-L. Chueh, E. Plis, S. Krishna, H. A. Bechtel, J. Guo, and A. Javey, Nano Lett. **11**, 5008 (2011).
[13]H. Takita, N. Hashimoto, C. T. Nguyen, M. Kudo, M. Akabori, and T. Suzuki, Appl. Phys. Lett. **97**, 012102 (2010).
[14]M. Z. Elias, Physica E **108**, 96 (2019).
[15]A. Ohtake, T. Mano, and Y. Sakuma, Sci. Rep. **10**, 4606 (2020).
[16]J. Wróbel, G. A. Umana-Membreno, J. Boguski, D. Sztenkiel, P. P. Michałowski, P. Martyniuk, L. Faraone, J. Wróbel, and A. Rogalski, Phys. Status Solidi **14**, 1900604 (2020).
[17]S. Kalem, J.-I. Chyi, H. Morkoç, R. Bean, and K. Zanio, Appl. Phys. Lett. **53**, 1647 (1988).
[18]Y. Tokura, T. Saku, S. Tarucha, and Y. Horikoshi, Phys. Rev. B **46**, 15558 (1992).
[19]R. S. Goldman, H. H. Wieder, K. L. Kavanagh, K. Rammohan, and D. H. Rich, Appl. Phys. Lett. **65**, 1424 (1994).
[20]P. Ramvall, N. Carlsson, P. Omling, L. Samuelson, W. Seifert, M. Stolze, and Q. Wang, Appl. Phys. Lett. **68**, 1111 (1996).
[21]S. Löhr, S. Mendach, T. Vonau, C. Heyn, and W. Hansen, Phys. Rev. B **67**, 045309 (2003).
[22]D. Ercolani, G. Biasiol, E. Cancellieri, M. Rosini, C. Jacoboni, F. Carillo, S. Heun, L. Sorba, and F. Nolting, Phys. Rev. B **77**, 235307 (2008).
[23]M. Akabori, T. Q. Trinh, M. Kudo, H. Hardtdegen, T. Schäpers, and T. Suzuki, Physica E **42**, 1130 (2010).
[24]G. Moschetti, H. Zhao, P. Nilsson, S. Wang, A. Kalabukhov, G. Dambrine, S. Bollaert, L. Desplanque, X. Wallart, and J. Grahn, Appl. Phys. Lett. **97**, 243510 (2010).
[25]L. Desplanque, S. E. Kazzi, J.-L. Codron, Y. Wang, P. Ruterana, G. Moschetti, J. Grahn, and X. Wallart, Appl. Phys. Lett. **100**, 262103 (2012).
[26]Y. Jeong, H. Choi, and T. Suzuki, J. Cryst. Growth **301–302**, 235 (2007).
[27]Y. Jeong, M. Shindo, H. Takita, M. Akabori, and T. Suzuki, Phys. Status Solidi C **5**, 2787 (2008).
[28]L. Ö. Olsson, C. B. M. Andersson, M. C. Håkansson, J. Kanski, L. Ilver, and U. O. Karlsson, Phys. Rev. Lett. **76**, 3626 (1996).
[29]H. Yamaguchi, R. Dreyfus, Y. Hirayama, and S. Miyashita, Appl. Phys. Lett. **78**, 2372 (2001).
[30]C. T. Nguyen, H.-A. Shih, M. Akabori, and T. Suzuki, Appl. Phys. Lett. **100**, 232103 (2012).
[31]S. P. Le, T. Ui, and T. Suzuki, Appl. Phys. Lett. **107**, 192103 (2015).
[32]T. Ui, R. Mori, S. P. Le, Y. Oshima, and T. Suzuki, AIP Adv. **7**, 055303 (2017).
[33]T. Suzuki, H. Ono, and S. Taniguchi, Sci. Technol. Adv. Mater. **6**, 400 (2005).
[34]J. Singh, *Electronic and Optoelectronic Properties of Semiconductor Structures* (Cambridge University Press, 2003).
[35]M. de Jong, W. Chen, H. Geerlings, M. Asta, and K. A. Persson, Sci. Data **2**, 150053 (2015).
[36]D. N. Quang, V. N. Tuoc, N. H. Tung, and T. D. Huan, Phys. Rev. Lett. **89**, 077601 (2002).
[37]D. N. Quang, V. N. Tuoc, N. H. Tung, and T. D. Huan, Phys. Rev. B **68**, 153306 (2003).
[38]D. N. Quang, V. N. Tuoc, and T. D. Huan, Phys. Rev. B **68**, 195316 (2003).
[39]M. Abrahams, J. Blanc, and C. Buiocchi, Appl. Phys. Lett. **21**, 185 (1972).
[40]K. L. Kavanagh, M. A. Capano, L. W. Hobbs, J. C. Barbour, P. M. J. Marée, W. Schaff, J. W. Mayer, D. Pettit, J. M. Woodall, J. A. Stroscio, and R. M. Feenstra, J. Appl. Phys. **64**, 4843 (1988).
[41]A. Bensaada, R. Cochrane, R. Masut, R. Leonelli, and G. Kajrys, J. Cryst. Growth **130**, 433 (1993).
[42]H. Sakaki, T. Noda, K. Hirakawa, M. Tanaka, and T. Matsusue, Appl. Phys. Lett. **51**, 1934 (1987).
[43]T. Saku, Y. Horikoshi, and Y. Tokura, Jpn. J. Appl. Phys., Part 1 **35**, 34 (1996).
[44]S. Cho, A. Majerfeld, A. Sanz-Hervás, J. J. Sánchez, J. L. Sánchez-Rojas, and I. Izpura, J. Appl. Phys. **90**, 915 (2001).
[45]J. J. Sánchez, J. I. Izpura, J. M. G. Tijero, E. Muñoz, S. Cho, and A. Majerfeld, J. Appl. Phys. **91**, 3002 (2002).
[46]S. Cho, A. Majerfeld, J. Sánchez, E. Munoz, J. Tijero, and J. Izpura, Microelectron. J **33**, 531 (2002).